SENSOR DATA FUSION ANALYSIS FOR HEO SPACE DEBRIS USING BAS^{3}E

Carlos Yanez[(1)], Juan Carlos Dolado[(2)], Alfredo Antón[(3)]

[(1)]GMV Innovating Solutions, 17 rue Hermès 31520 Ramonville St. Agne, France
[(2)]CNES, 18 av. Edouard Belin 31401 Toulouse Cedex 9, France
[(3)] GMV, Isaac Newton 11, 28760 Tres Cantos, Spain
e-mail: cyanez@gmv.com, juan-carlos.doladoperez@cnes.fr, amanton@gmv.com

ABSTRACT

This paper describes an application using BAS^{3}E, a simulation tool developed by French Space Agency (CNES) in collaboration with GMV, focused on the performance analysis of different space surveillance networks in the detection and cataloguing of a HEO population of objects. The use of BAS^{3}E is described, including the concatenation of computation stages, the databases management and the persistence layers. Sensor networks considered within this study contain different combinations, in quantity and quality, of ground-based telescopes and radars. These sensor networks have been selected attending to criteria such as viable number of stations for a mid-term deployment and quality (measurement noise, observability constraints …) in line with already-operating sensors. This study tends to evaluate the advantages of fusing data from different sources (only optical measurements, or optical measurements along with radial distance and/or radial velocity data) concerning HEO orbit determination and, besides, conclusions are presented on the gain of incorporating additional sensors in a hypothetical space surveillance system ground network.

Index Terms— Space Situational Awareness, space debris, HEO objects, sensor fusion

1. INTRODUCTION

One of the main missions of a Space Surveillance system is the detection and cataloguing of space objects having a size compatible with the detection constraints of its sensors. While radars are used to observe objects placed at Low Earth Orbits (LEO), and telescopes to observe objects orbiting in Medium (MEO) and Geostationary Orbits (GEO), for objects orbiting in Highly Elliptical Orbits (HEO), both types of sensors are suited for observations. In particular, the passage through the perigee can be observed from radar stations, while in the high-altitude orbit portion telescopes are intended to be the source of observations. In this way, combining data derived from different type of sensor seems advantageous for tracking HEO objects.

BAS^{3}E (*Banc d'Analyse et de Simulation d'un Système de Surveillance de l'Espace*) is a space surveillance system simulation bench that includes the "real world" simulation (objects and sensors) and the operational surveillance system (e.g. catalogue maintenance, sensor planning, collision risk assessment, re-entry prediction and fragmentation detection). This tool enables the performance analysis of the surveillance network depending on its features, as well as the algorithms involved in the catalogue maintenance, analysis and planning systems.

This paper is organized as follows. Section II gives a description of the simulator employed within this study. Test case scenarios are defined in Section III including the objects population and different sensors used. Section IV contains the visibility analysis of sensors, both independently or joint in surveillance networks. Performance on orbit determination is presented in Section V along with a comparison between Least square method (LSM) and Extended Kalman filter (EKF) results. Finally, Section VI is devoted to conclusions and perspectives of further work.

2. BAS^{3}E

BAS^{3}E is a simulation tool conceived and developed for the design and analysis of space surveillance systems. This concept of space surveillance takes into account, among others, the following activities:

- Detection, tracking and generation of observations of space objects,
- Object identification and tracking correlation,
- Orbit determination,
- Maintenance of a space debris catalogue,
- Collision risk analysis with operational satellites or with other space debris,
- Fragmentation detection,
- Reentry assessment.

The first activity mentioned above is performed by a physical network of sensors, either on-ground or space-based, that allows us to obtain observations of different kinds, such as angular position, distance or radial velocity. The rest of activities correspond to a software system that identifies and treats the tracking data coming from the

sensors network and compute an orbit of the space object more or less accurate in order to perform the relevant analysis thereafter.

From the information technology point of view, BAS^{3}E is a simulation bench of distributed computation, coded in JAVA language and that relies on two main libraries, both developed by CNES:

- PATRIUS: celestial mechanics library
- ALIS: simulation bench infrastructure: Man-machine interface (MMI), data persistence handling modules (SQL and XML), computation executions…

This JAVA coding enable BAS^{3}E to make advantage of a set of technologies such as:

- Eclipse : development infrastructure,
- Hibernate: SQL database persistence system,
- XStream: XML files persistence system,
- OSGI: modularization of applications,
- MAVEN: building software procedure and dependencies management.

From a user point of view, BAS^{3}E is composed of three main products:

- BAS3E-IHM: with the simulator MMI, preferences management, simulation context,
- BAS3E-RMS: Runtime Machine Service, which is the simulator core, simulator execution engine,
- BAS3E-CRS: Cluster Runtime Service, which is the execution client in a cluster computation. It is launched automatically by the RMS in the context of a stage execution.

This project structure relies on the BAS3E-COMMON project that contains all high-level classes which are specific to the simulator, along with simulation objects and stages and the computation algorithms.

In a simulation context, the user shall define a certain number of simulation objects and stages. Simulation objects refer to common or particular simulation configurations such as forces model, atmosphere configuration, filters to select objects from the database… Simulation stages usually contain the computation interval and a set of simulation objects. Simulation stages can be run either on stand-alone or on the cluster and they can be concatenated by means of the different persistence layer. For example, the propagation stage takes the nearest state vector to the computation start epoch of the objects (eventually selected by a filter) from the objects SQL database. The stage is executed with the forces model and integration configuration defined in the simulation objects. As an output, this stage will provide binary files containing the propagated orbits. This output could be used thereafter as an input to the visibility opportunities stage, which, jointly with the sensors SQL database (containing sensor measurement types, sensor location, visibility constrains, sensor quality…), will generate a binary file format containing the periods of time where the objects can be observed for a given sensor.

The simulation of a space surveillance system leads to massive number of calculation that could be performed in parallel in different cores or machines. From the beginning, BAS^{3}E has been designed and developed for parallel computing in, for instance, a High Performance Computing (HPC) service. Results of the present study have been obtained by using a CNES own HPC service, which is dedicated to scientific projects demanding a great computing and processing capacity.

3. TESTS SCENARIOS DEFINITION

The initial population of objects is the 2009 ESA-MASTER population database of objects larger than 10 cm in or crossing the LEO region. It is composed of 20811 objects, from which we have extracted 2139 orbiting in HEO applying constrains on the minimum and maximum altitudes. In particular,

- Maximal perigee altitude = 600 km
- Minimal apogee altitude = 10000 km

These constraints lead to orbits with an eccentricity higher than 0.4. HEO objects can be divided into groups depending on the inclination (see Figure 1). A first group appears for inclinations lower than 10 deg and it is generally composed of rocket stages launched from French Guiana. A second group between 20 and 30 deg corresponds to rocket stages launched from Cape Canaveral. Similarly, a third group of objects around 50 deg that is mainly composed of rocket stages launched from Baikonur and, finally, the fourth group between 60 and 70 deg with objects that are/have been in a Molniya orbit.

Reference orbits for a 6-days interval are computed with a numerical propagator including the following forces:

- Earth potential up to 12th order and 12th degree.
- Drag force with MSIS2000 model for atmospheric density.
- Luni-solar perturbations.
- Solar Radiation Pressure.

Objects orbiting along these eccentric orbits can be observed both by telescopes and radars. Locations for these sensors have been chosen attending to criteria such as deployment viability and visibility performance (see Table 1). Indeed, sites for the telescopes are those of already-operating TAROT telescopes [1]. Concerning radars, low latitude locations have been favored in order to maximize visibility periods around the perigee. Three types of sensors are considered, one telescope and two radars (either range radar or Doppler radar), whose measurement qualities are defined in Table 2 in terms of one parameter, the standard deviation of the Gaussian noise.

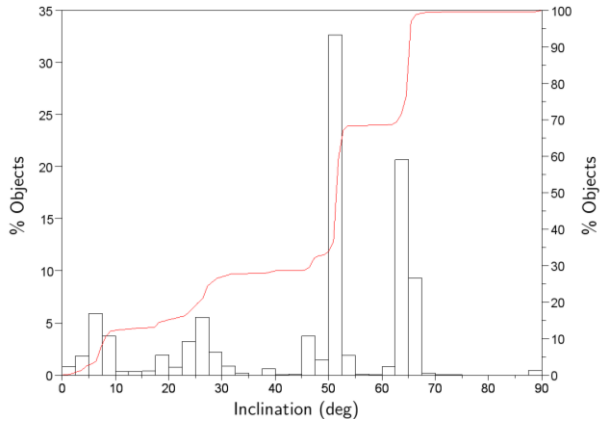

Figure 1 : Percentage of HEO objects depending on the inclination. Histogram refers to the values at the left and the red solid line representing the accumulated percentage refers to the values at the right.

Telescopes are considered to take measurements every 30s whereas this time span is reduced to 5s for radars. Observations are possible provided that all the visibility constraints are fulfilled. For telescopes, we take into account:

- Object elevation : within 0 and 90 deg,
- Object azimuth : without constraint,
- Object distance : further than 20000 km,
- Night: angle between the zenith and the Sun between 113 and 180 deg,
- Illumination: object is illuminated by the Sun.

Regarding radars:

- Object elevation : within 0 and 90 deg,
- Object azimuth : without constraint,
- Object distance: between 100 and 2000 km.

We consider several on-ground surveillance networks with different number of telescopes and radars. The composition of each surveillance network is detailed in Table 3. Notice that radars will be all considered either Range or Doppler ones, so we analyze, in total, 11 surveillance networks.

4. VISIBILITY ANALYSIS

Once the objects and sensors databases are defined in BAS^{3}E and reference orbits are computed and stored in binary files, we can run the visibility opportunities stage. Results from this computation stage are post-processed in order to obtain different visibility statistics that enables us to compare the surveillance networks in terms of visibility performance. We focus the analysis in three aspects: how often and how long an object can be seen and how many objects are simultaneously in the field-of-view of a sensor.

Type	Name	Longitude (deg)	Latitude (deg)	Altitude (m)
Telescope	TCA	6.924 E	43.752 N	1270.0
Telescope	TCH	70.732 W	29.261 S	2347.0
Radar	Fr. Guiana	52.772 W	5.209 N	0.0
Radar	Reunion	55.456 E	21.328 S	0.0
Radar	Fr. Polynesia	149.416 W	17.768 S	0.0
Radar	Gabon	9.465 E	0.419 N	0.0

Table 1 : Geodetic position of the surveillance stations

Measurement type	Radar Distance	Radar Doppler	Telescope
Angular	10.0 mdeg	10.0 mdeg	3.0 mdeg
Radial distance	10 m	-	-
Radial velocity	-	1 m/s	-

Table 2 : Measurement noise applied to each sensor type.

Name	Composition
0T4R	Fr. Guiana + Reunion + Fr. Polynesia + Gabon
2T0R	TCA + TCH
2T1R	2T0R + Fr. Guiana
2T2R	2T1R + Reunion
2T3R	2T2R + Fr. Polynesia
2T4R	2T3R + Gabon

Table 3 : Surveillance networks composition

4.1. Visibility opportunities

Figure 2 presents the evolution of the visibility opportunities per day of the objects population depending on the surveillance network. The point at the Y-axis represents the percentage of objects that are not accessible for a given surveillance network in the 6-days interval. For instance, approximately 5% of objects are not observed even with the complete network (2T4R). The curves are read as follows. If we take the point 20% of objects corresponding to the complete network, we obtain roughly 2 visibility opportunities per day, that is to say, 20% of the objects can be observed by the complete network at least twice per day, or, equivalently, 80% of the population can be observed more often than twice per day. It is important to note the asymptote that reaches the curve corresponding to the complete network at the bottom-left of the figure. This means that all the visible objects can potentially be seen at least once per day.

For radars individually, we conclude from our study a dependence on the latitude for the percentage of population that is accessible. In the case of radars installed near the equator (French Guiana and Gabon) around 35% of objects do not fulfil the visibility constraints, whereas this percentage increases up to 45% for radars in higher latitudes (Reunion and French Polynesia).

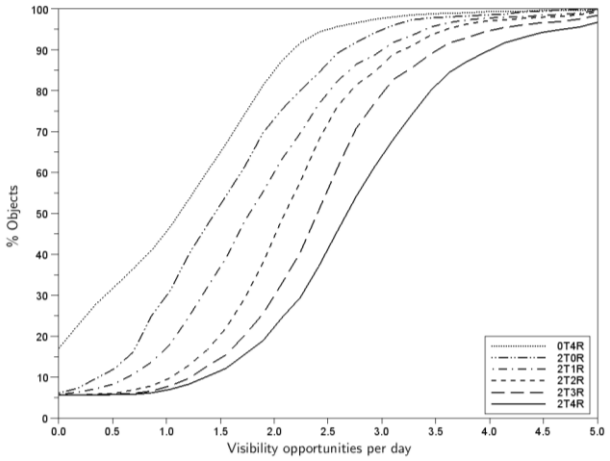

Figure 2 : Visibility opportunities per day.

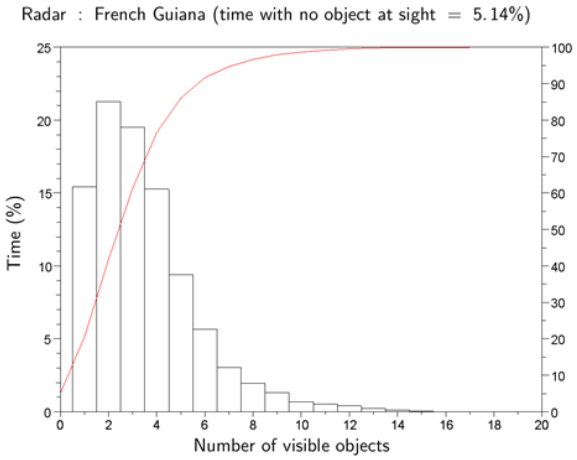

Figure 3 : Sensor load of a radar located at French Guiana.

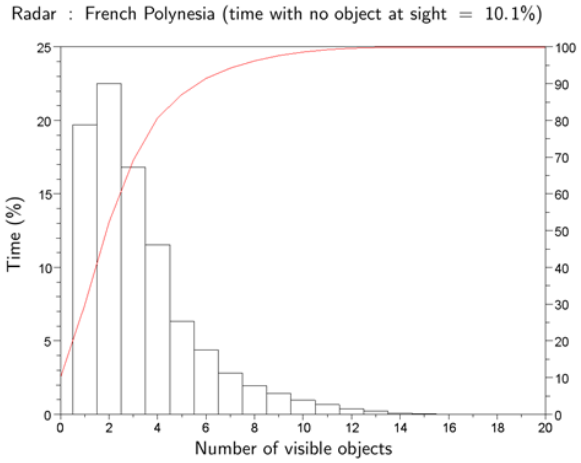

Figure 4 : Sensor load of a radar located at French Polynesia.

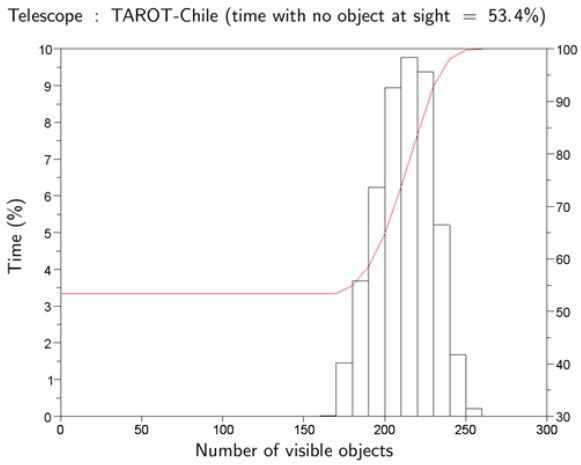

Figure 5 : Sensor load of a telescope located at Chile. Histogram refers to the values at the left and the red solid line representing the accumulated percentage refers to the values at the right.

4.2. Visibility duration

The four radars present similar results for the visibility duration of an observation. The mode lies within 5 and 7 minutes. On the other hand, telescopes have much longer visibility periods which are enabled by the slower apogee passage. The mode for an observation duration stays within 0.5 and 1.5 hours.

4.3. Sensors load

In this study sensors are considered to be surveillance one. No pointing strategy is defined to track the sky. Thus, field-of-view constraint does not apply in the capability of observing an object, and only constraints defined in section 3 are taken into account. This fact leads to a population of simultaneous visible objects that are far beyond the capabilities of actual sensors technologies for taking measurements to all of them.

In that way, results that follow, especially in orbit determination performance, should be understood as the probability of reaching a certain confidence on the object state vector if the given surveillance network tracks preferentially this object during six days.

Sensor load in the case of the four radar locations is similar, being between 1 and 4 the number of objects accessible to the radar most of the time. Difference between radars is again related to the latitude location and it concerns the percentage of time that no object is at sight. For radars installed near the equator this blinded time represents around 5% of total time, whereas this percentage increases up to 10% approximately for higher latitude locations (see Figure 3 and Figure 4).

Concerning telescopes load, we can see in Figure 5 the case of a telescope located at Chile. Between 200 and 250 objects are accessible for this telescope and similar figures

are found for the other location. Obviously, day-night cycle plays a major role in the visibility periods and we can notice that Chile telescope is blinded 53.4% of the time and France telescope, by his side, is blinded 70.4% of the time. These percentages are fully justified by the simulation epoch (early May) and the latitudes of both locations.

5. ORBIT DETERMINATION PERFORMANCES

In this section we present the orbit determination performances of the different space surveillance networks in terms of the covariance obtained at the end of the estimation interval process, that is to say, the covariance associated to the final state vector.

Six days observation data is processed either with a batch filter (Least Square Method [2]) or a sequential filter (Extended Kalman Filter [2]).

Forces model used in the orbit determination differs from the one used in the reference orbit computation and, therefore, from the one used in computing sensor observations. This difference, which is reduced to a lower accuracy on the earth potential (order and degree 6 instead of 12) and the lack of solar radiation pressure modelling, simulates somehow the inaccurate knowledge of real forces acting on space debris.

Initial state vector is not perturbed but we consider that our knowledge of initial state vector is not perfect through an associated initial covariance. 1-sigma values of this initial covariance are set to 10, 5 and 5 km in position for the three directions of the TNW frame, respectively; and, in an analogous way, to 10, 5 and 5 m/s in velocity.

5.1. Least Square Method

We present hereafter results on the final covariance in position for the tree directions of the TNW frame.

5.1.1. Along –track direction

Figure 6 shows the results of surveillance networks containing Doppler radars on the direction parallel to the velocity that is usually the direction for which the uncertainty is larger. It is worth noting the curves corresponding to 0T4R and 2T2R networks since they are composed of the same number of sensors. This figure indicates that sensor data fusion, coming from optical and radar sensors, reduces the uncertainty on the state vector of HEO objects more than a network with all observations coming from the same type of sensor, Doppler radar in this case. The gain is similar to the one obtained when two more radars are added to the surveillance network (2T4R case).

Figure 7 presents the same curves but, this time, concerning surveillance networks that contain range radars.

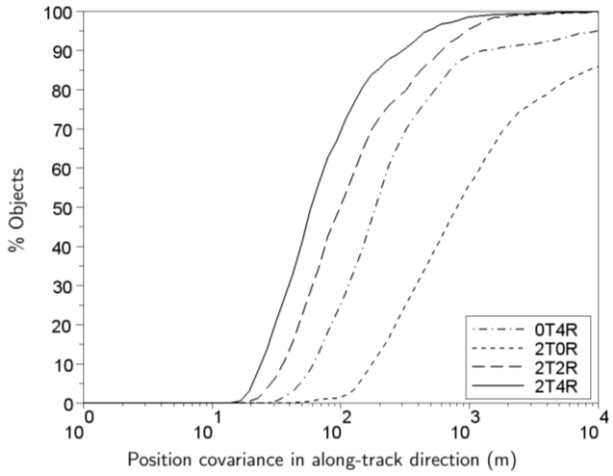

Figure 6 : Position covariance in along-track direction at the end of the orbit determination time span. The percentage of objects is accumulative and only concerns common visible objects for all the surveillance networks. Radar stations are Doppler ones.

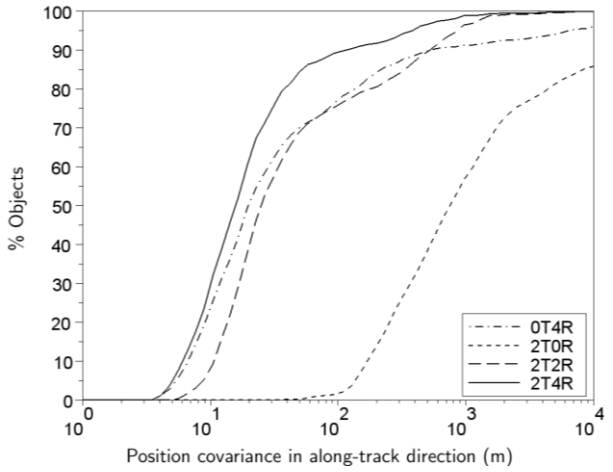

Figure 7 : Position covariance in along-track direction at the end of the orbit determination time span. The percentage of objects is accumulative and only concerns common visible objects for all the surveillance networks. Radar stations are range ones.

It is important to notice that, when range radars are considered, the decrease on the uncertainty of the state vector does not always come as a consequence of sensor data fusion. On the contrary, 0T4R provides better results that 2T2R for the objects whose orbit is more accurately known (covariance < 50m). This fact is explained by a higher performance of range radars compared to Doppler ones in this study, in other words, noise values considered for both types of radars do not provide a similar accuracy. Indeed, all curves where range radars take part are shifted towards the left compared to Doppler ones (cf. Figures 6 and 7).

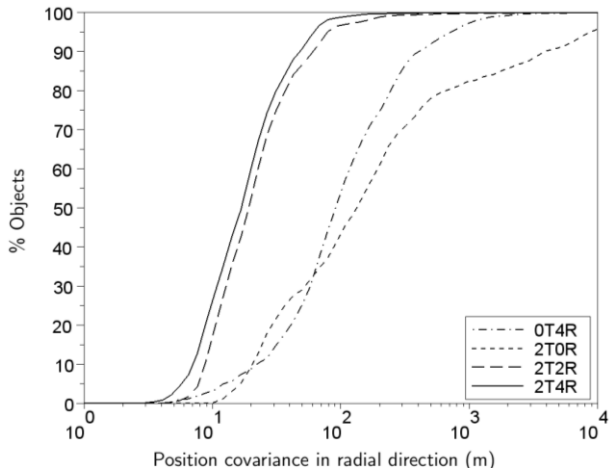

Figure 8 : Position covariance in radial direction at the end of the orbit determination time span. Radar stations are Doppler ones.

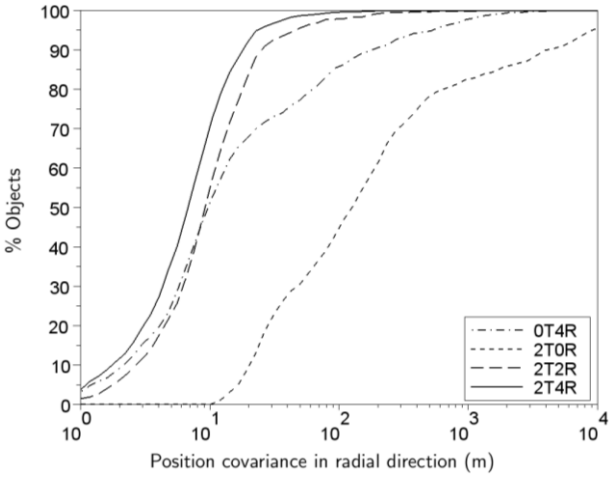

Figure 9 : Position covariance in radial direction at the end of the orbit determination time span. Radar stations are Range ones.

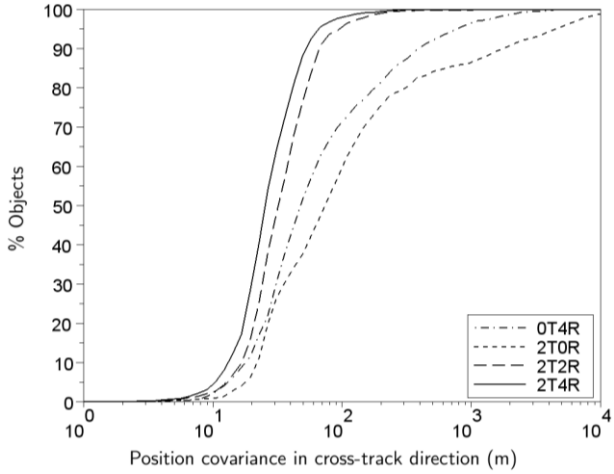

Figure 10 : Position covariance in cross-track direction at the end of the orbit determination. Radar stations are Doppler ones.

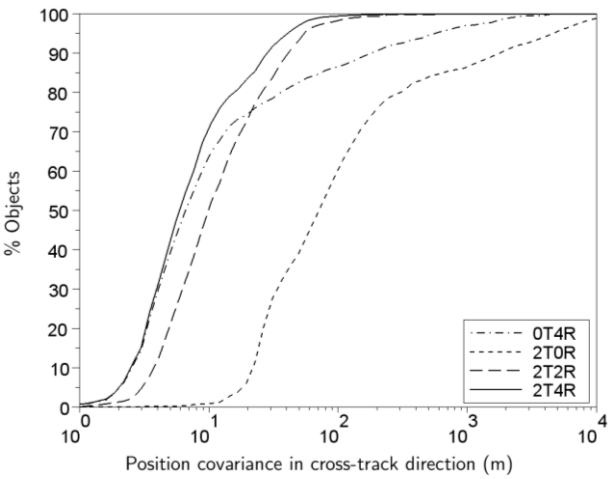

Figure 11 : Position covariance in cross-track direction at the end of the orbit determination. Radar stations are Range ones.

Moreover, as it can be seen in Figure 7, the more accurate orbits are obtained thanks to range radar measurements. This suggests that, for noise levels considered in our study, there is a region with along-track covariance lower than 100 m in which the accuracy is mainly driven by range measurements, and telescopes extra-information does not improve more the state vector knowledge. However, sensor data fusion provides an improvement on orbital accuracy for less accurate orbits. Indeed, the 2T2R surveillance network allows reaching almost 100% of the population with along-track covariance lower than 1km, whereas this percentage decreases to 90% for 0T4R. It is worth noting that this region stays within telescopes best accuracies obtained, and, therefore, we can state that for this test case when accuracies of both types of sensor becomes comparable, sensor data fusion helps in reducing the uncertainty on the state vector.

5.1.2. Radial and cross-track directions

Figure 8 presents the position covariance obtained in the case of Doppler radars. It is remarkable the increased accuracy reached with the 2T2R surveillance network compared to the 0T4R. For instance, there are 25% of objects with a position covariance smaller than 50m with the 0T4R network and, for this same value in the covariance, the percentage increases up to 85% in the case of 2T2R, highlighting the advantages of sensor fusion data.

For the case of surveillance networks containing range radars (see Figure 9), we observe again that the orbits which are more accurately estimated (position covariance of the order of meters) come mainly from the information provided by radar measurements. In a similar way as in along-track direction results, sensor data fusion is advantageous in the

range of accuracies that are accessible for both telescopes and radars.

Figures 10 and 11 present results in cross-track direction. The behavior is similar to the one observed in radial direction with both range and Doppler radars.

5.1.3. Covariance representativity

Taking advantage of having simulated the real world and, in consequence, the fact that reference orbits are known, we can compute the error in position and in velocity committed in the estimated orbits and compare it with the uncertainty given by the covariance. In all cases covariance underestimates the error committed and therefore the achievable orbit determination accuracy inferred by the covariance is too optimistic. The reason is that systematic errors due to unmodeled forces are not taken into account in the covariance matrix computation. The way to overcome this discrepancy lies in estimating parameters associated to unmodeled or bad-known forces in order to take into account these uncertainties in the orbit determination process.

5.2. Extended Kalman Filter

The same orbit determination scenarios have been executed with an extended Kalman filter (EKF). This type of filter can have numerical difficulties when processing a large amount of observations if the covariance matrix and the Kalman gain become very small. That situation is interpreted by the Kalman filter as a situation in which the knowledge on the object trajectory is accurate enough and, in consequence, no correction on the state vector is needed any more. In other words, last estimation is preponderant over any information coming from the sensors. In that way, error introduced by a difference in dynamical models, for instance, is not corrected and moreover it will increase in the propagation. This will lead the problem to get out of the linearity region and, therefore, results from EKF can diverge. This problematic can be prevented in a simple way by adding an additional term in each propagation step to the covariance matrix in order to avoid it to become too small. This additional term, called process noise term [2], accounts for uncertainties caused by systematic forces and measurement model errors. In this study, a simplified description of the process noise matrix has been used, which is defined by one parameter: the process noise associated to position errors (Q). A parametric study is carried out in order to determine the optimal value of this parameter. Figure 12 presents results on the convergence of the EKF depending on the value of Q for several surveillance networks. A trend is observed in the way of improving the convergence with increasing values of Q (as explained before) up to a point when this convergence worsens. This behavior is explained by the following consideration.

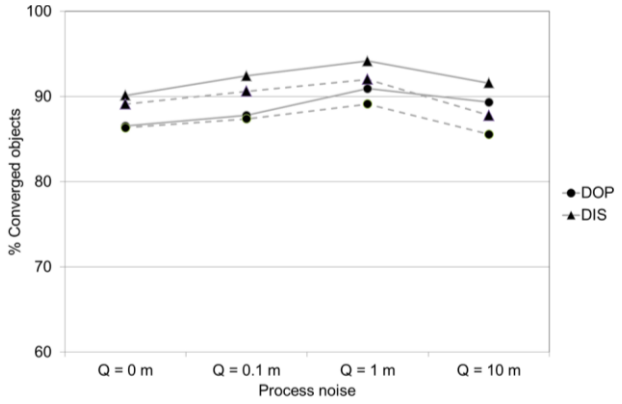

Figure 12 : Percentage of converged object in the orbit determination process using EKF depending on the value of the process noise parameter. Solid lines correspond to the 2T4R surveillance network and dashed line to the 2T2R one.

Process noise term cannot be increased indefinitely. Indeed, an upper bound is found when process noise is too large. This derives into a situation where last estimation is not trusted and sensor information coming from the last observation is always considered more important than previous one. Information provided by past observations is then somehow lost and this leads to a higher sensitivity with respect to errors in measurements and therefore larger state vector corrections. The problem can then get out of the linearity region and diverges. Therefore, attending to Figure 12 an optimal value of Q around 1m is found for these study scenarios. Besides, this value is confirmed if we compare state vector errors with the associated covariance. Covariance found in the case Q=1m is better in agreement with state vector errors than in the other cases. In an operational case, where real observation are processed, the choice of the process noise parameter is trickier since we do not know the error committed; the choice is then based on numerical stability of the filter and considerations on the order of magnitude of neglected forces.

A comparison has been made between results obtained with LSM and EKF. If process noise is not considered in EKF, results from both methods are rather similar, as it can be expected.

6. CONCLUSIONS

BAS^{3}E is a modular and flexible tool developed by the CNES in collaboration with GMV that enables to perform a large variety of simulations with the aim of analyzing the capabilities and performance of space surveillance systems in different scenarios.

In the study presented in this paper, BAS^{3}E is used for analyzing the advantages of sensor data fusion in the orbit determination of objects orbiting in highly eccentric orbits.

A visibility analysis is performed for the considered sensors (telescopes and radars) individually and grouped into networks. Information on the quantity, duration and frequency of observations as well as sensor load statistics are provided. In addition to this analysis, orbit determination performances are analyzed for both a batch and a sequential filter, discussing the benefits of space surveillance networks composed of different type of sensors, that is to say, the sensor data fusion.

7. REFERENCES

[1] M. Laas-Bourez et al., A new algorithm for optical observations of space debris with the TAROT telescopes, Advances in Space Research, 44 (11), 1270-1278 (2009).

[2] O. Montenbruck and E. Gill, Satellite Orbits. Models, Methods and Applications. Springer-Verlag Berlin Heidelberg (2000).